Jurnal Tribologi 17 (2018) 40-64

Jurnal Tribologi
Website : jurnaltribologi.mytribos.org
e-issn: 2289-7232

Investigation a unique scratching of the failure mechanisms of the coatings with TiN thin layers deposited on 316L stainless steel

Lucian Capitanu [1], Liliana-Laura Badita [2,*], Virgil Florescu [3]

[1] Institute of Solid Mechanics of the Romanian Academy, Bucharest 010141, ROMANIA.
[2] National Institute of Research and Development for Mechatronics & Measurement Technique, Bucharest 021631, ROMANIA.
[3] University of Civil Engineering, Bucharest 050153, ROMANIA.
[*]Corresponding author: badita_l@yahoo.com

KEYWORD

SS 316L
Pulse Laser Deposition
TiN coatings
SPSI scratch test
critical events

ABSTRACT

Starting from the finding that the coatings with TiN of the total hip prostheses femoral heads made of Ti-6Al-4V alloy have tendencies to wear (abrasive, adhesive or bio-tribo-corrosion), the paper has proposed to establish the failure mechanisms of these thin layers coatings. For economic reasons, the studies were made on TiN coatings on 316L stainless steel (SS 316L), steel with mechanical characteristics similar to the Ti-6Al-4V alloy. Three types of TiN coatings were made on cylindrical samples of SS 316L by the Pulse Laser Deposition (PLD) method. Depending on the number of deposition pulses, coatings with different thicknesses and harnesses were obtained. Since the failure of coatings is generally due to the failure of coating's adhesion to the substrate's material, the coating's adhesion was tested by single pass single indenter (SPSI) scratch tests to completely avoid the occurrence of the fatigue phenomenon that may occur in the case of multi-pass single indenter (MPSI) scratch test or multi-pass dual indenters (MPDI). The critical failure events of the three types of coatings were highlighted and commented, concluding that PLD coatings with 10000 and 20000 pulses are the ones that offer the most favorable perspectives from the coating – substrate adhesion point of view.

Received 31 July 2017; received in revised form 30 August 2017; accepted 15 November 2017.
To cite this article: Lucian et al. (2018). Investigation a unique scratching of the failure mechanisms of the coatings with TiN thin layers deposited on 316L stainless steel. Jurnal Tribologi 17, pp.40-64.

1.0 INTRODUCTION

Tribosystem friction properties depend strongly on the properties of materials, the external environment and the nature of the wear particles generated during sliding (Liu et al., 2004; Kustas et al., 2007; Molinari et al., 1997; Fouquet and Pichon 2004; Lanning and Wei 2004; Liu et al., 2003; Santos et al., 2006; Österle et al., 2008; Wilson et al., 1999; Bemporal et al., 2008; Avelar-Batista et al., 2006; Zhang et al., 2008; Varenberg et al., 2002). The way a surface is deformed, will dictate the nature of the wear particles generated, which in turn can significantly influence the wear behavior of materials.

The tribofilms and wear particles generated during sliding are known to influence the behavior of the friction materials (Zhou et al., 2007). Tribological mechanisms describe the macro-mechanical friction and wear phenomena by taking into account the distribution efforts – strains in the entire contact, total elastic and plastic deformations, formation process of the wear particles and its dynamics (Holmberg, 1992; Holmberg et al., 1998). Recently, the effect of different mating materials on friction behavior of TiN coatings with different crystallographic orientations was analyzed (Tanno and Azushima, 2009). It was noted that the formation of a titanium oxide layer on the surface leads to a lower value of friction. Much research has been aimed at studying the tribological behavior of pure titanium metal and titanium alloys (Vidal and Muñoz, 2008; Chelliah and Kailas, 2009). But reports on the wear behavior of Ti thin layers are rare. Since titanium nitrides are hard biocompatible materials (Coll et al., 1998; Rie et al., 1995; Pellman, 2000) with excellent resistance to abrasion, more advanced processing methods have been developed in order to achieve a nitrided layer on the surface of materials.

At the nitriding in plasma, nitrogen atoms diffuse into the titanium matrix, forming a layer of TiN and Ti_2N compounds, usually followed by a deeper diffusion layer (Yibas et al., 1995). This layered structure produces a continuous profile of hardness, thus providing adequate support of the coating (Rie et al., 1995; Yilbas et al., 1996). However, the physical properties of treated surface are highly dependent on plasma coating technique and processing parameters. Excellent corrosion resistance of titanium alloys resulted in the formation of a stable protective oxide film very strongly adhered to metal surfaces (Schutz, 2005). On the other hand, the corrosion resistance of TiN can be affected by its structural defects – holes, pores and small cracks (Ylbas et al., 1995). In fact, Meletis et. al., 1986, showed that an adequate structure without defects and dense TiN film can significantly improve corrosion resistance.

Co-Cr-Mo alloy is one of the most used implant alloys for artificial joints and offers a good combination of mechanical properties, corrosion resistance and biocompatibility (Schultz, 2005). There are several types of Co-Cr-Mo materials currently used. Each material has a different microstructure and thus different properties optimized for specific design or function (Büscher et al., 2004; Julian and Munoz, 2011; Sims, 1972; Rodrigues et al., 2011). During the manufacture of alloys with high carbon content (HC), carbon precipitates to form relatively large spherical inclusions, carbide in metal-crystalline matrix, which divides the hardness, strength and wear. For the mass composition of this alloy, carbides with the highest metal-carbon ratio are favored, such as Cr and Mo matrix to form Cr21-Mo2-C6. As a consequence, the matrix immediately surrounding the inclusions of carbide is poor in chromium.

This was suggested as areas for increased corrosion of the surface (Sims, 1972). Indeed, the microstructure and alloy composition affect the corrosion behavior in simulated body fluids due to changes in surface chemistry. Hiromoto et al. (2005), observed that the passive film composition depends on the solution chemistry and limits grain growth, results in a decrease of corrosion resistance of weak alloys forged Ni-Co-Cr-Mo. It is also well known that these

microstructural properties changes affect the mechanical and wear properties (Hiromoto et al., 2005; Jacobs et al., 1990; Cawley et al., 2003). Dobbs and Robertson (1983) analyzed the mechanical properties and hardness of a Co-Cr-Mo alloy heat-treated and have found a correlation between carbide volume fractions and wear rate, but they have not noticed any effect on mechanical properties. Similarly, they showed that heat treatment improved the mechanical properties of the alloy, without loss of corrosion resistance.

It is very clear that TiN hard coatings of the Ti-6Al-4V alloy femoral heads increase their surface hardness, but there are many cases in which these coatings are damaged by flaking or scratching. The causes may be multiple, depending on the material characteristics, cover properties, type and technological parameters of coating process, the mechanical loading, etc.

2.0 EXPERIMENTAL PROCEDURE

Investigation of a number of 18 modular total hip prostheses, of which 10 of Co-Cr alloy and 8 of Ti-6Al-4V alloy recovered as a result of some replacement surgeries following the femoral head's failure, has occasioned the attempt to establish the failures cause. Figure 1 shows images obtained by optical microscopy of some relevant worn areas on the surface of the femoral head one of the femoral heads recovered, from Ti-6Al-4V coated with TiN. Based on the analysis of the optic microphotographs presented below, an ample discussion on the causes of the TiN coating's failure from the Ti-6Al-4V femoral head can be made. It is about the appearance of some corrosion pits – Figure 1 (a) and (b), the partial removal of the coating and its plastic flow due to the contact with hard particles – Figure 1 (c) and (d) and of the fatique phenomenon of the coating – Figure 1 (e) and (f) and of the Ti-6Al-4V substrate abrasion by the wear particles and probably bone or bone cement residues. The causes of such failures may be based on a poor adhesion of the TiN coating to the Ti-6Al-4V substrate.

To investigate in detail the adhesion of coating to substrate, for economic reasons, TiN coatings have been deposited on 316L stainless steel (SS 316L) substrates, cheaper but with mechanical characteristics similar to the Ti-6Al-4V alloy.

TiN depositions were realized by physical laser deposition (PLD) method, inside a deposition chamber, with stainless steel reaction chamber at 5000, 10000 and 20000 pulses, using a KrF* excimer source, COMPexPro 205 type (λ = 248 nm, $\tau_{FWHM} \approx$ 25 ns, ν = 10 Hz) running at a repetition frequency of 10 Hz. The laser beam was incident at 45^0 on the target surface.

TiN commercial tablets from Plasmaterials (99.5% purity, 1" diameter and 0.250" thick) were used as targets for depositions, while cylindrical samples made of SS 316L stainless steel (10.2 mm diameter and 6 mm thick), with hardness of 150 HV30 were used as substrates for coatings. The substrate samples had the surfaces polished with sandpaper with increasing granulation, from 200, 400 to 600. They were subjected to hardness measurements on a universal hardness and microhardness tester LECO LV. Disk samples were placed parallel with targets (on geometric axis), at 5 cm separation distance, in front of them. Laser fluency on the target surface was ~ 4.8 J/cm^2 at an energy of 500 mJ. The detailed description of the method is presented elsewhere (Capitanu et al., 2015).

After the coatings deposition, both the thickness and the micro-hardness of the coatings were measured. To determine the thickness of TiN thin layers, cross sections of the SS 316L steel samples, on which the coatings were deposited, were realized. These cross sections, polished with sandpaper with 400, 600, 800, and 1200 granulation, were analyzed after coating with optical microscopy, Atomic Force Microscopy (AFM) and Scanning Electron Microscopy (SEM). This is

because even if the surface quality of the slif (polished cross-section of the sample) is very good, determining the thickness of the deposited layer is quite difficult. SEM images (magnification 250x) of TiN coating thickness for samples of (a) 5000, (b) 10000 and (c) 20000 pulses are shown in Figure 2.

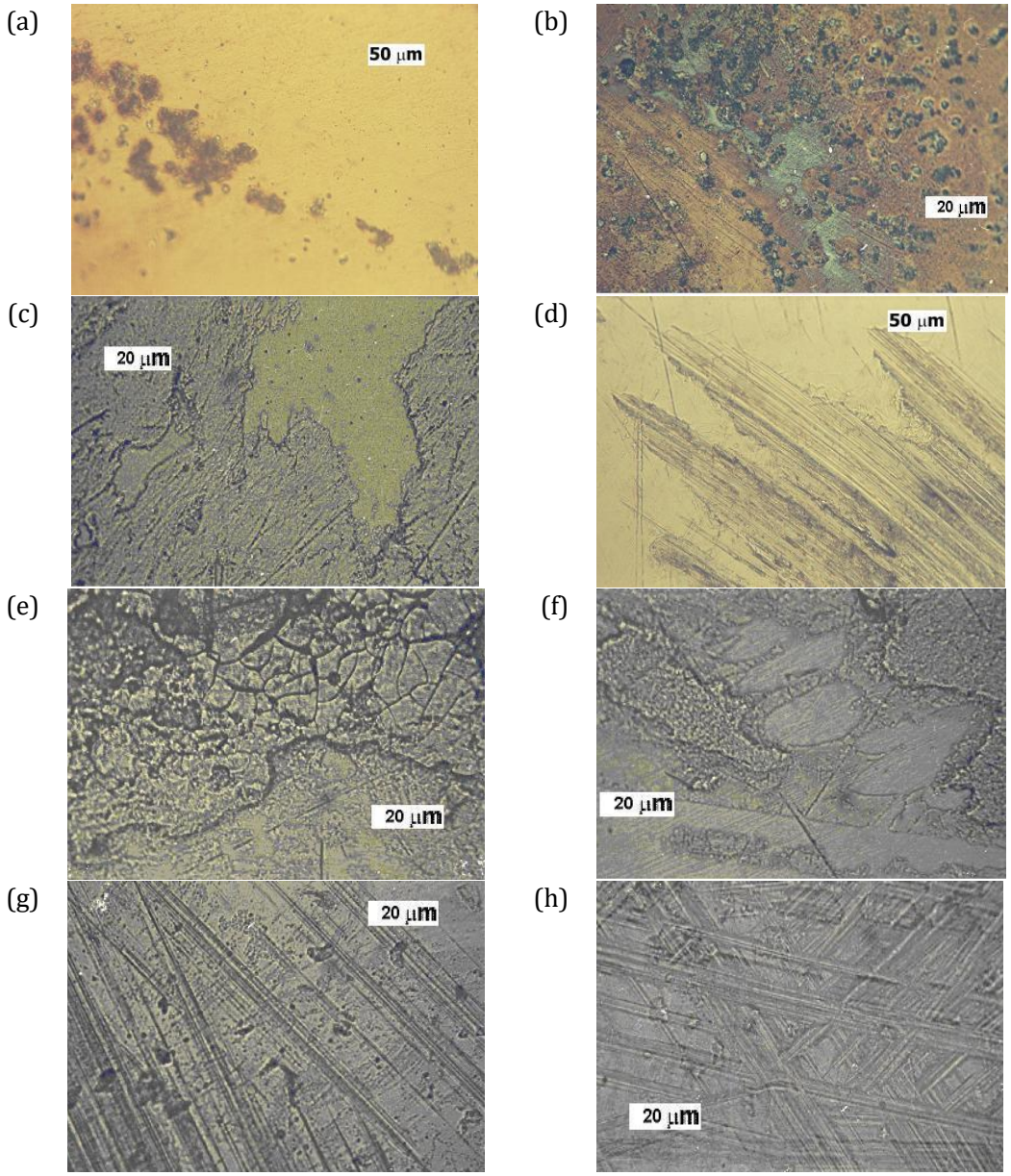

Figure1: Images obtained by optical microscopy of some worn areas of TiN coatings on the Ti-6Al-4V femoral heads, recovered as a result of some replacement surgeries.

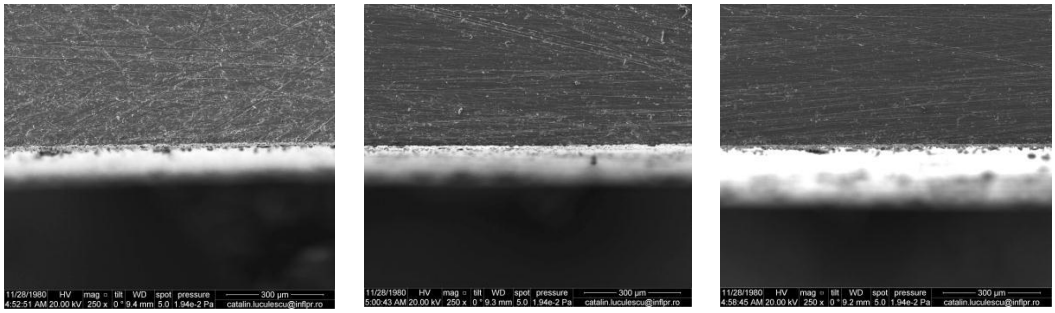

Figure 2: SEM images (magnification 250x) of TiN coatings thickness for 5000, 10000 and 20000 pulses samples.

The coatings thickness, measured by SEM on the cross sections, was 1.62 μm at 5000 pulses, 2.11 μm at 10000 pulses and 2.72 μm at 20000 pulses. Average values of substrate and TiN coatings hardness were established. The HV_5 values of the substrate's hardness were 287, 420 and 464, respectively, for the samples coated at 5000, 10000 and 20000 pulses, respectively, while the $HV_{0.5}$ values of the coatings microhardness were 349, 539 and 738 $HV_{0.5}$, respectively. An increase of the coating – substrate composite hardness is observed with the increase in the layers thickness and accordingly, with the increase in the number of pulses. Thus, it is possible that the uniformity of deposited layers to occur as a result of coating with a thicker layer of defects existing on the substrate (with a larger thickness for the sample of 20000 pulses).

3.0 INVESTIGATION BY UNIQUE SCRATCHING OF FAILURE MECHANISMS OF THE TiN PLD COATINGS ON STAINLESS STEEL

In order to verify the adhesion between the coating and the substrate, three different scratch test modes (Gore and Gates, 1997) are generally used, which are schematically shown in Figure 3, both to evaluate the abrasion resistance of the coating-substrate composite, and to observe the failure mechanism, as follows:

(a) Single pass single indenter (SPSI) scratch test: a single scratch pass of the clean steel sample surface, with a large indenter (R = 100 μm, cone angle 120^0) at different loads of 1 N, 3 N, 5 N, 10 N, 15 N, 20 N, 25 N and 30 N, respectively, leading to the conditions schematically shown in Figure 3 (a).

(b) Multi-pass single indenter (MPSI) scratch test: multiple passes (10 passes) scratch the fresh surface of the steel sample over the same track, with a large indenter (R = 100 μm, cone angle 120°) at different loads of 1 N, 5 N, 10 N, 15 N, 20 N, 25 N and 30 N, respectively, leading to the conditions schematically shown in Figure 3 (b).

(c) Multi-pass dual indenters (MPDI) scratch test, which leads to the conditions shown schematically in Figure 3 (c) consists of three steps: 1) Pre-scratching of the flat surface of the steel with the same big multi-pass indenter (10 passes); 2) Pre-scanning to follow the profile of the central region of the scratch line with the small indenter (R = 5 μm, cone angle 60^0) at a very low load of 0.03 N, without causing further damages or deformations.

(d) Finally, scratching with the same small indenter using a fixed load of 0.3 N in the central region of the scratch track created by the large multi-pass indenter. The sliding track with the small indenter was at the center of the scratching path made by the large indenter and covered the

equilibrium state of the wear path created by the large indenter. The intention of pre-scratching with the large indenter is to create the pre-deformed surface layer similar to the one produced in the real abrasion process.

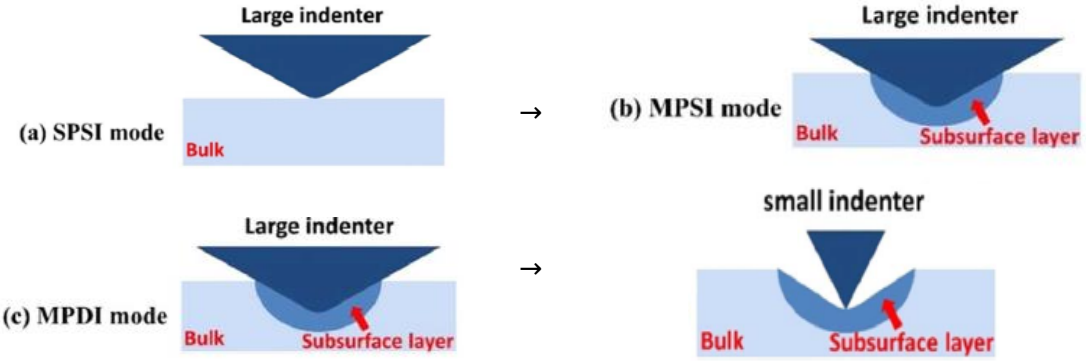

Figure 3: A schematic representation of conditions perpendicular to the scratch direction: (a) SPSI scratch mode; (b) MPSI scratch mode; (c) MPDI scratch mode (Adapted from Gore and Gates, 1997).

In this paper, the single-pass scratch test was used to verify the adhesion between coating and substrate. The loads applied were in the range of (2.5 - 125) N. The use of a natural diamond friction coupling against the material to be investigated allows a considerable simplification of the testing device. The movement is, in this case, a pure sliding movement, common in many tribometers with continuous or alternative motion, and the sample being tested is a circular plate (disk), with a diameter of 10.2 mm and a thickness of 6 mm.

The scratch test was performed under the following conditions:

(a) Constant loading;
(b) loads: 2.5 N, 5 N, 10 N, 20 N, 40 N, 80 N and 125 N;
(c) radius of inderter's tip: 2 mm;
(d) indenter's material: diamond;
(e) scratching speed: 1 cm/min;
(f) scratch length: 1 cm.

Specific parameters of the sample of the coating-substrate system include:

(a) hardness and roughness of the substrate;
(b) hardness and roughness of the coating;
(c) coating's thickness.

The average roughness's R_a of TiN coatings surfaces were measured after scratching tests using atomic force microscopy (AFM). R_a values of 34.569 nm, 42.309 nm and 16.591 nm, respectively, were measured at a force of 2.5 N for coatings at 5000, 10000 and 20000 pulses, respectively.

After scratch tests performed, the surfaces of SS 316L steel disks coated with TiN were studied macroscopically and microscopically. The means for determining the critical load was microscopic and SEM observations. Because black-and-white SEM images of the scratches did not allow a proper qualitative characterization of the scratch tracks, the images recorded by optical microscopy were used for this.

4.0 RESULTS AND DISCUSSION

In Figure 4 are presented 3 samples studied after they were subjected to scratch testing. The distance between the scratches was 1 mm, not to change the wear mechanism due to the interaction between the adjacent scratches.

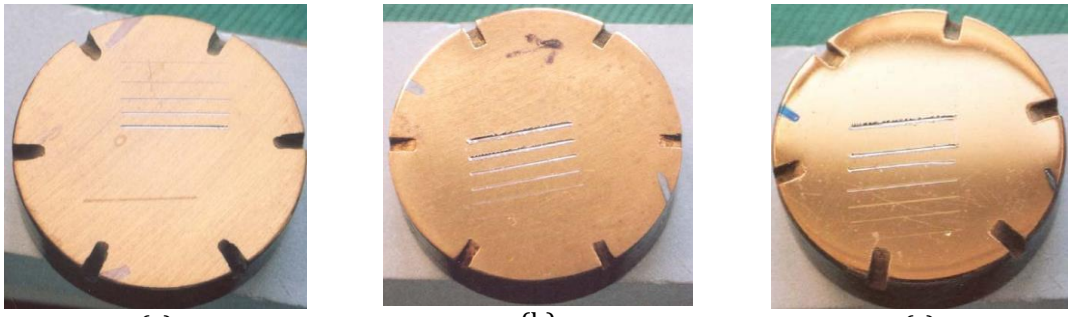

(a) (b) (c)

Figure 4: Macroscopic images of the SS 316L steel samples coated with TiN at (a) 5000 pulses, (b) 10000 pulses, (c) 20000 pulses, after the scratch tests.

Obtained scratches were photographed and their widths measured (usually at the beginning of the scratch, in the middle and at its end). Also, the cross sections of the scratching tracks were measured and recorded. Figure 5 shows optical microscopic images of tracks resulting after the scratch tests for the 5000 pulses sample, Figure 6 shows microscopic images of tracks resulting after the scratch tests for the 10000 pulses sample, and Figure 7 shows microscopic images of tracks resulting after the scratch tests for 20000 pulses sample.

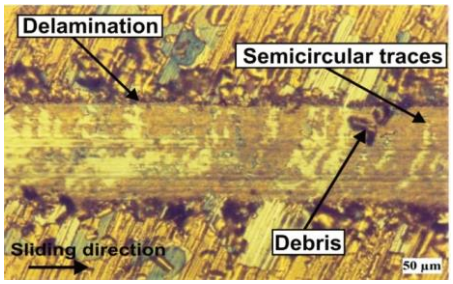

5000 pls, F = 2.5 N, track 1, pathway, 3.5 mm

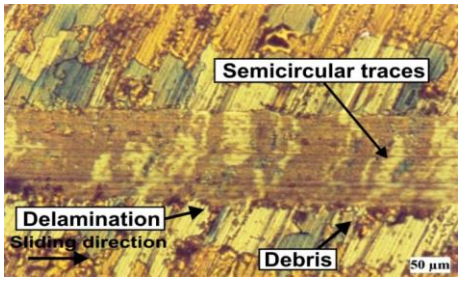

5000 pls, F = 2.5 N, track 1, pathway, 1 mm

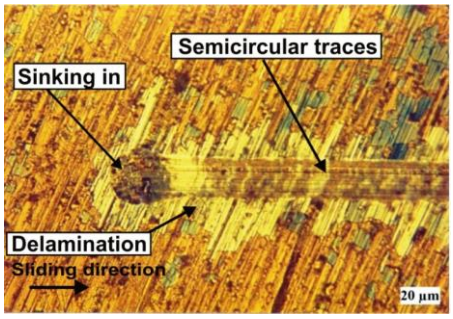

5000 pls, F = 2.5 N, track 1, start

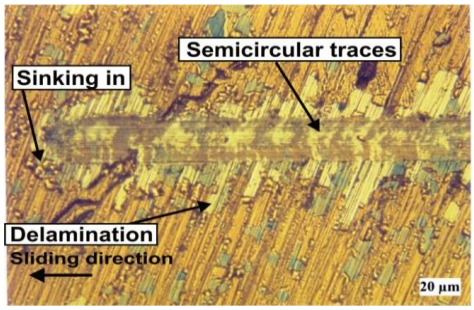

5000 pls, F = 2.5 N, track 1, final

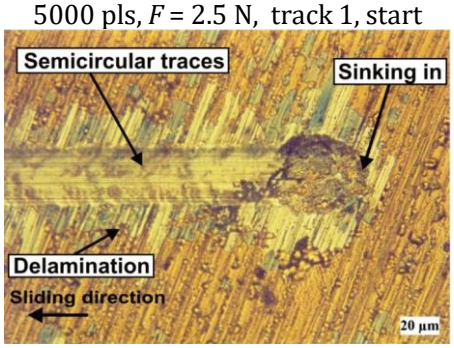

5000 pls, F = 5 N, track 2, start

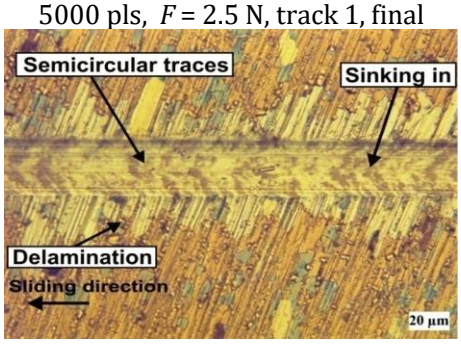

5000 pls, F = 5 N, track 2, pathway

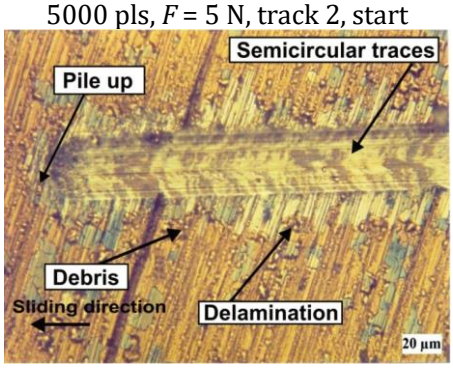

5000 pls, F = 5 N, track 2, final

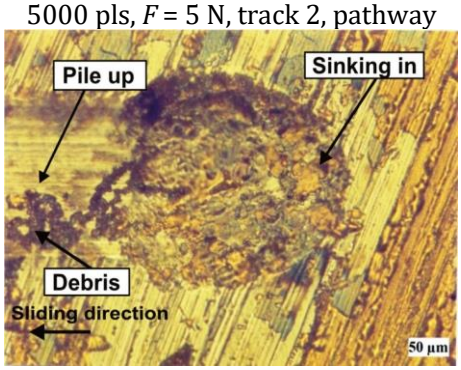

5000 pls, F = 5 N, track 2, start

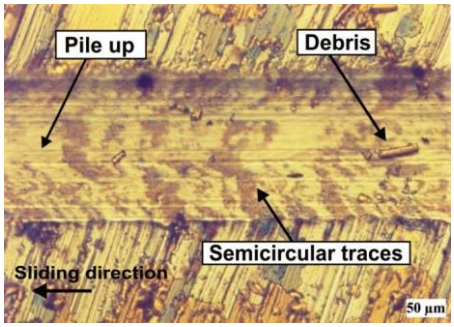

5000 pls,, F = 5 N, track 2, pathway

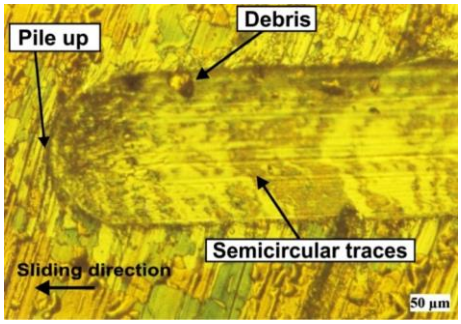

5000 pls, F = 5 N, track 2, final

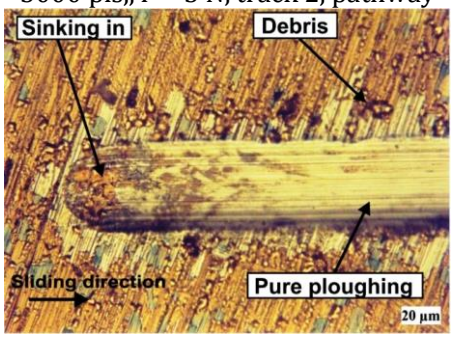

5000 pls, F = 10 N, track 2, start

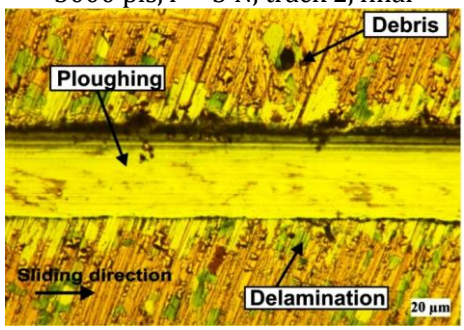

5000 pls, F = 10 N, track 3, parhway, 3 mm

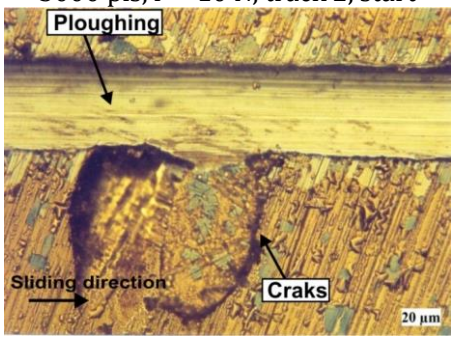

5000 pls, F = 10 N, track 3, pathway, 7 mm

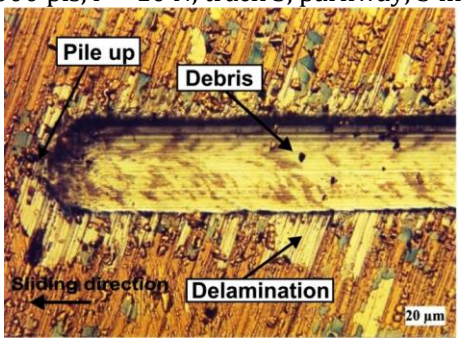

5000 pls, F = 10 N, track 3, final

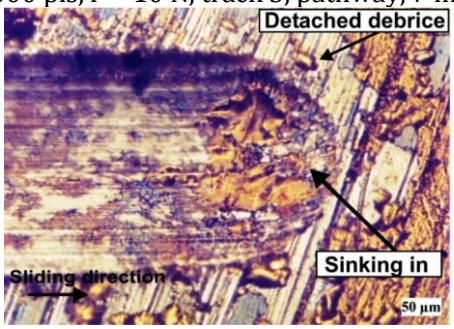

5000 pls, F = 10 N, track 3, start

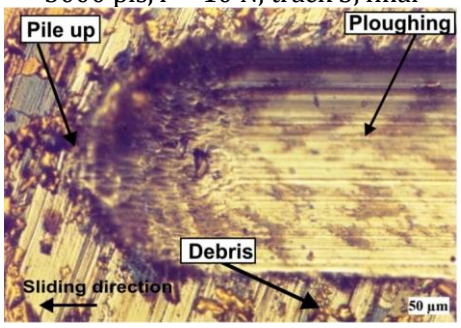

5000 pls, F = 10 N, track 3, final

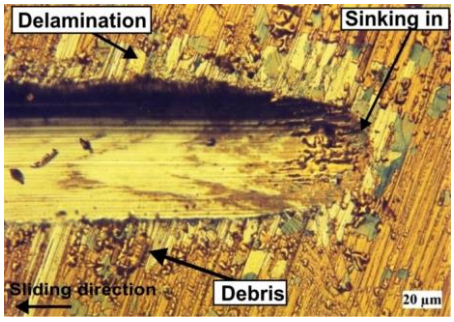

5000 pls, F = 20 N, track 4, start

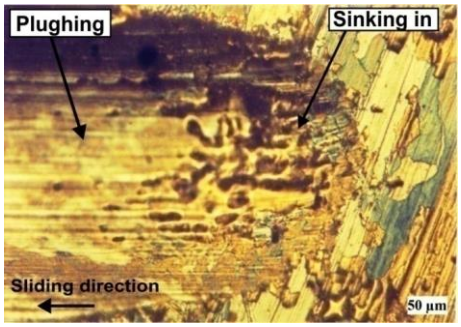

5000 pls, F = 20 N, track 4, start

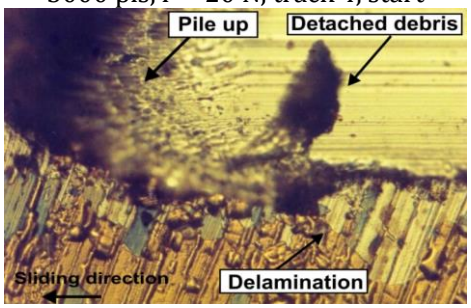

5000 pls, F = 20 N, track 4, final

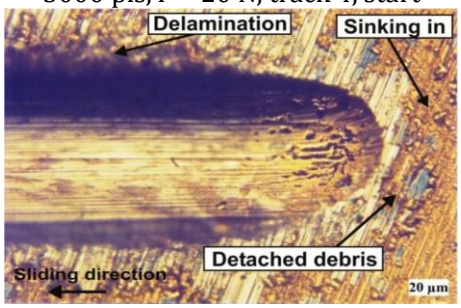

5000 pls, F = 40 N, track 5, start

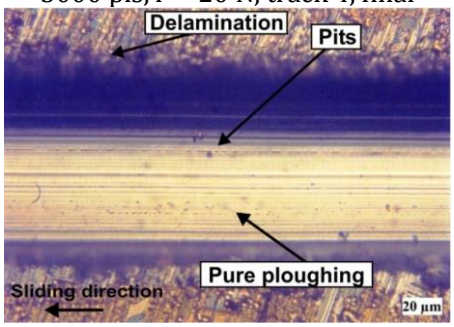

5000 pls, F = 40 N, track 5, pathway

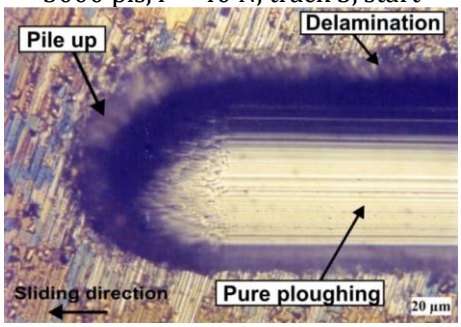

5000 pls, F = 80 N, track 6, final

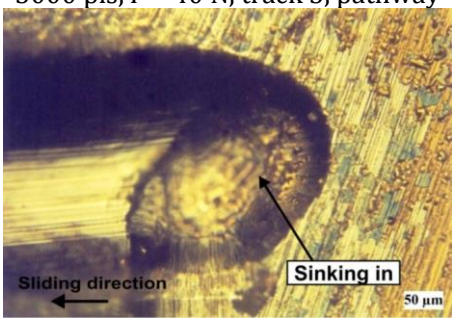

5000 pls, 25 x 20 = 500 x, F = 80 N, track 6, start

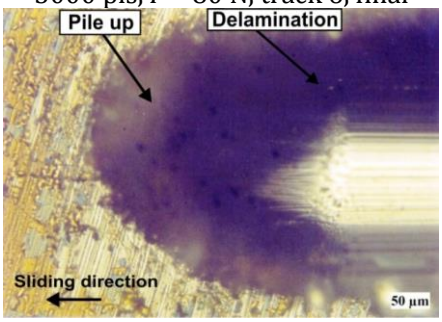

5000 pls, 25 x 20 = 500 x, F = 80 N, track 6, final

Figure 5: Microscopic images of the tracks produced after the scratch tests for the 5000 pulses sample.

Figure 6 shows collages at magnification 200x of the scratch tracks achieved at 2.5 N, 5 N, 10 N, 20 N, and 40 N load on the coating of 5000 pulses. At 80 N, the TiN coating at 5000 pulses was completely removed.

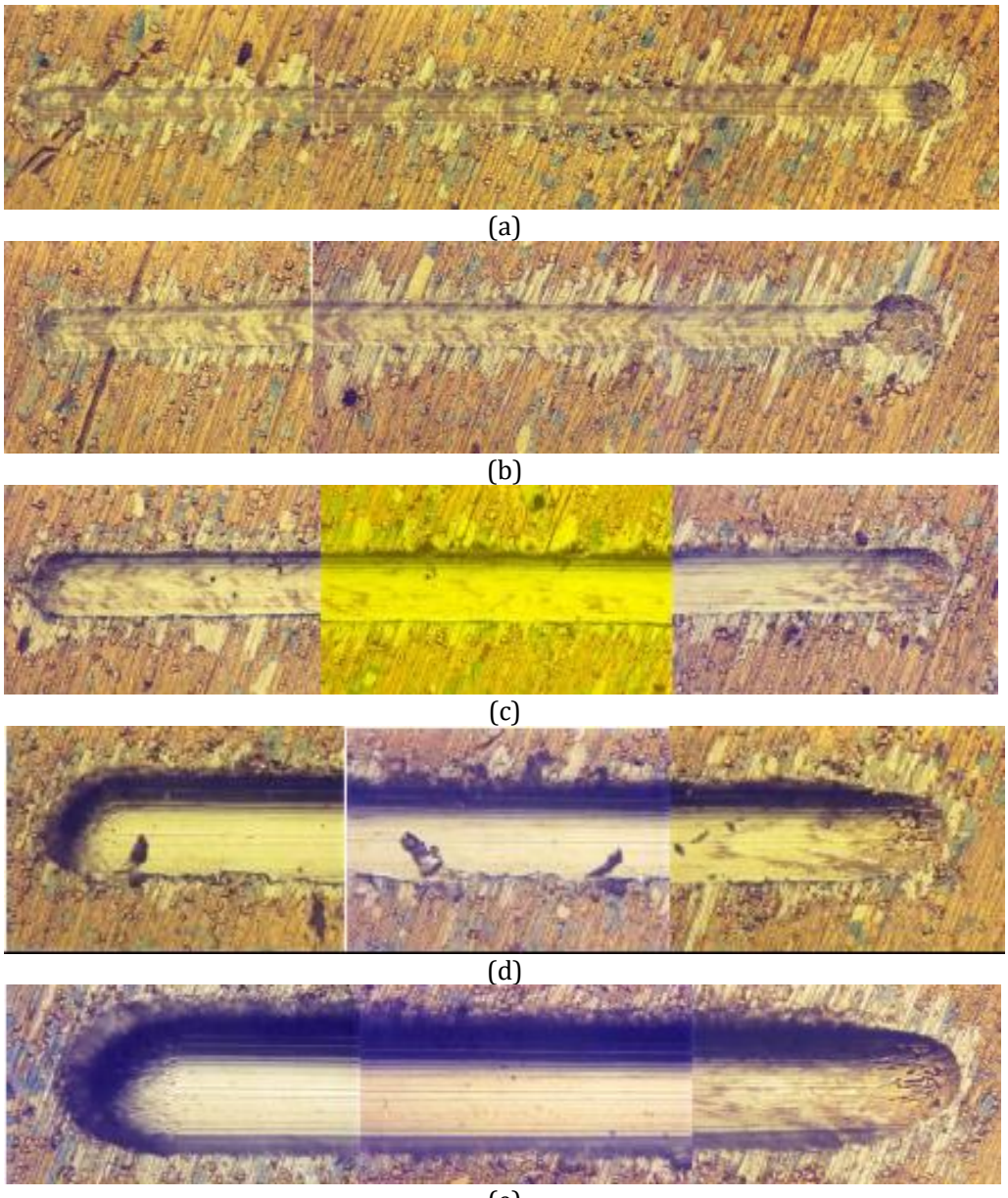

(a)

(b)

(c)

(d)

(e)

Figure 6: Collages of scratch tracks taken at 2.5 N (a), 5 N (b), 10 N (c), 20 N (d) and 40 N (e) loads on coating at 5000 pulses.

Analyzing the images of scratches at different loads on the coating with 5000 pulses, we can note the following common critical events, namely: delamination at the edge of the scratch, the appearance of worn remnants embedded in the wear track, but also the particles detached outside the track, the sinking in at the beginning of the scratch – as a result of the sudden application of the scratch load, pile–up at the end of the scratch, dimples and pits, semi-circular tracks on the bottom of the scratches. The intensity of these phenomena increases with increasing the load applied to scratching. These findings were made for a value of 349 $HV_{0.5}$ of the TiN coating for samples coated at 5000 pulses.

Two common aspects has to be noted to all scratches and for coatings made at 5000 pulses. When the indentor penetrates the coating surface, even at the smallest scratching loads used in this work, a shrinking in of the surface of the substrate – coating composite takes place. This phenomenon is manifested with an increased intensity, at the increasing of the scratch load.

At the end of the scratch, the piling up phenomenon of the material removed from the scratch path always occurs, with different intensity. In general, the piling up phenomenon manifests itself more strongly at higher loads. But, as will be seen later, this phenomenon is diminished if no accumulation of the worn material occurs on the scratching pathway, but this is removed as wear during the scratching process.

Although obvious, these two phenomena cannot be quantitatively quantified, and they can only be highlighted qualitatively, as was done in the present experiment, for the images shown in Figures 5 - 10.

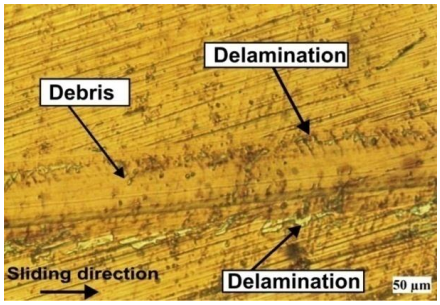

10000 pls, *F* = 2.5 N, track 1, pathway

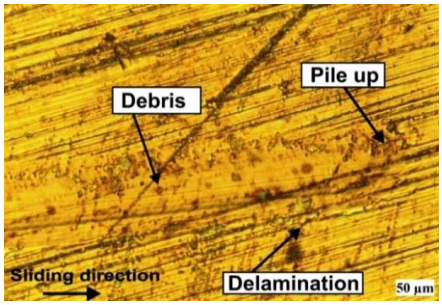

10000 pls, *F* = 2.5 N, track 1, final

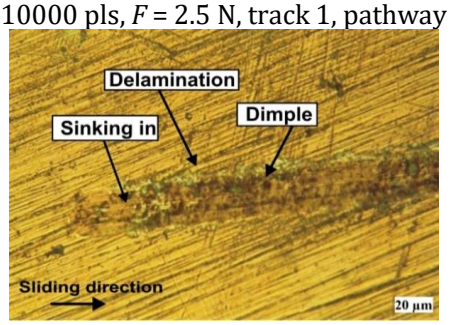

10000 pls, *F* = 5 N, track 1, start

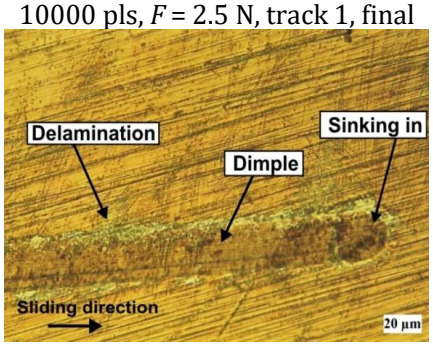

10000 pls, *F* = 5 N, track 2, pathway + final

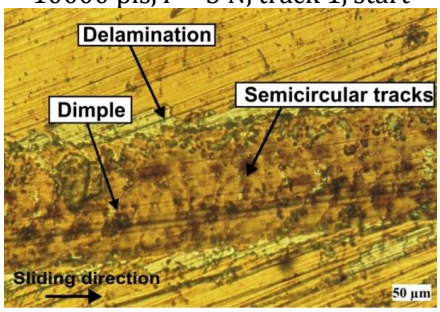

10000 pls, *F* = 5 N, track 2, pathway

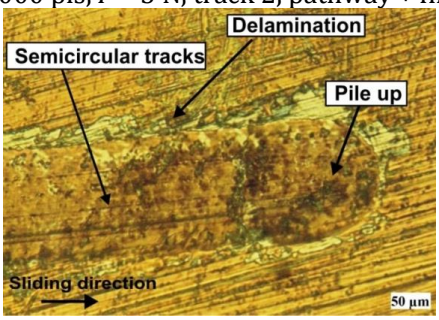

10000 pls, *F* = 10 N, track 3, final

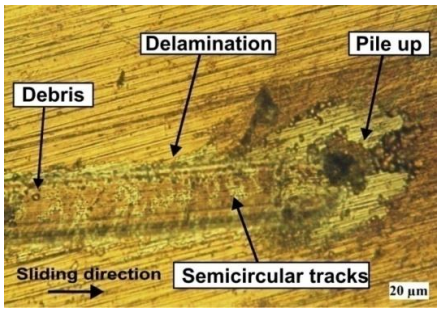

10000 pls, *F* = 10 N, track 3, pathway + final

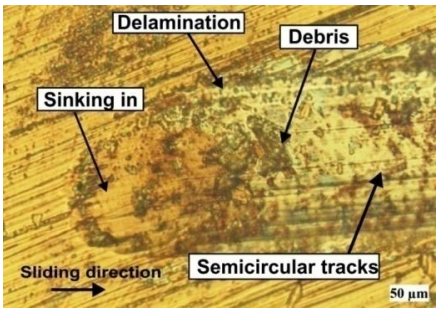

10000 pls, *F* = 10 N, track 3, start

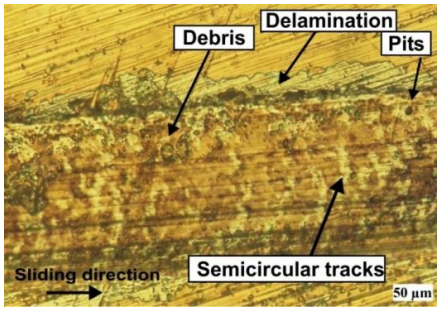

10000 pls, *F* = 10 N, track 3, pathway

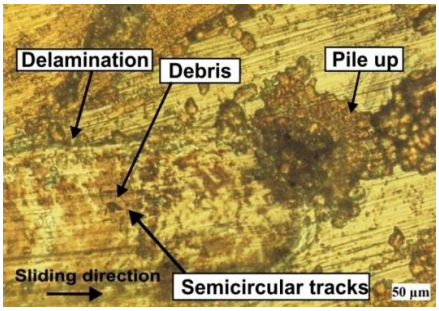

10000 pls, *F* = 10 N, track 3, final

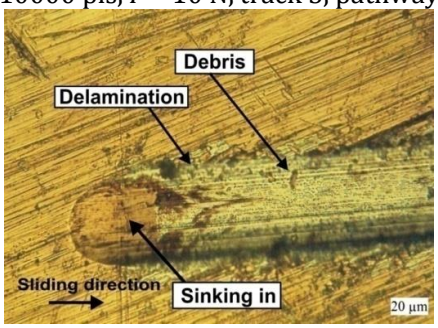

10000 pls, *F* = 20 N, track 4, start

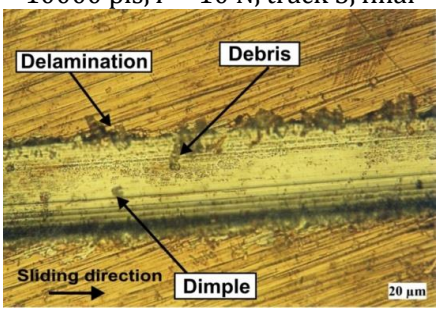

10000 pls, *F* = 20 N, track 4, pathway, 1.5 mm

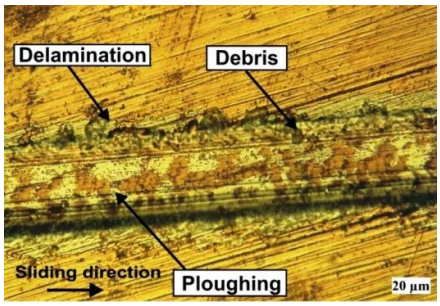

10000 pls, *F* = 20 N, track 4, pathway, 4 mm

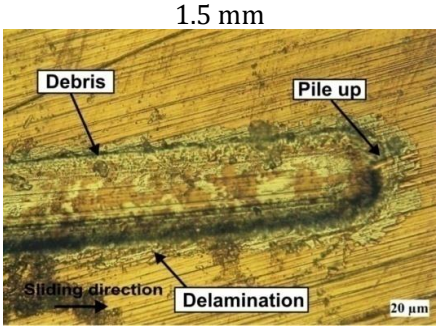

10000 pls, *F* = 20 N,track 4, final

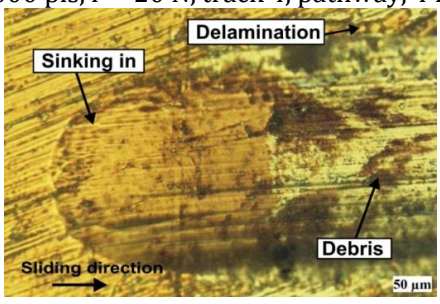

10000 pls, *F* = 20 N, track 4, start

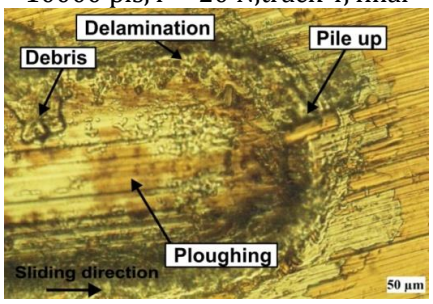

10000 pls, *F* = 20 N, rack 4, final

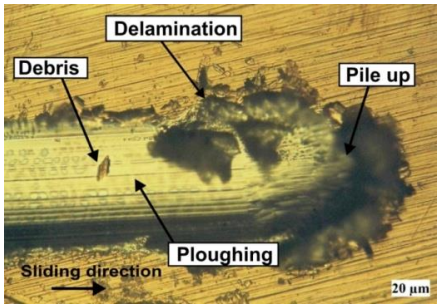

10000 pls, F = 40 N, track 5, final

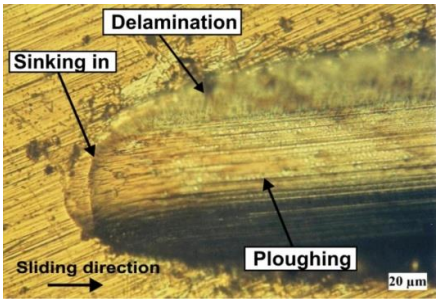

10000 pls, F = 80 N, track 6, start

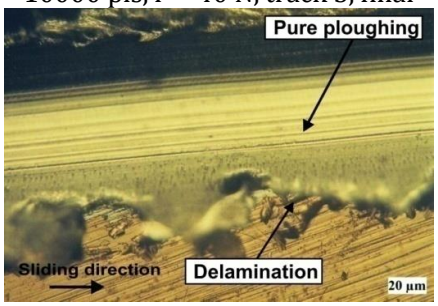

10000 pls, 25 x 8 = 200 x, F = 80 track 6, pathway

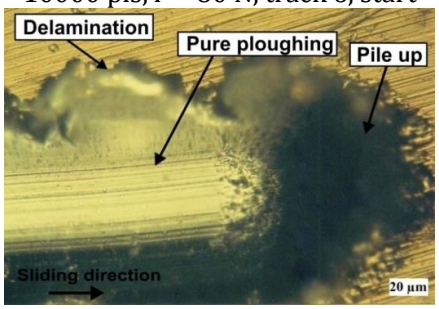

10000 pls, 25 x 8 = 200 x, F = 80 N, track 6, final

Figure 7: Microscopic images of the tracks produced after the scratch tests for the 10000 pulses sample.

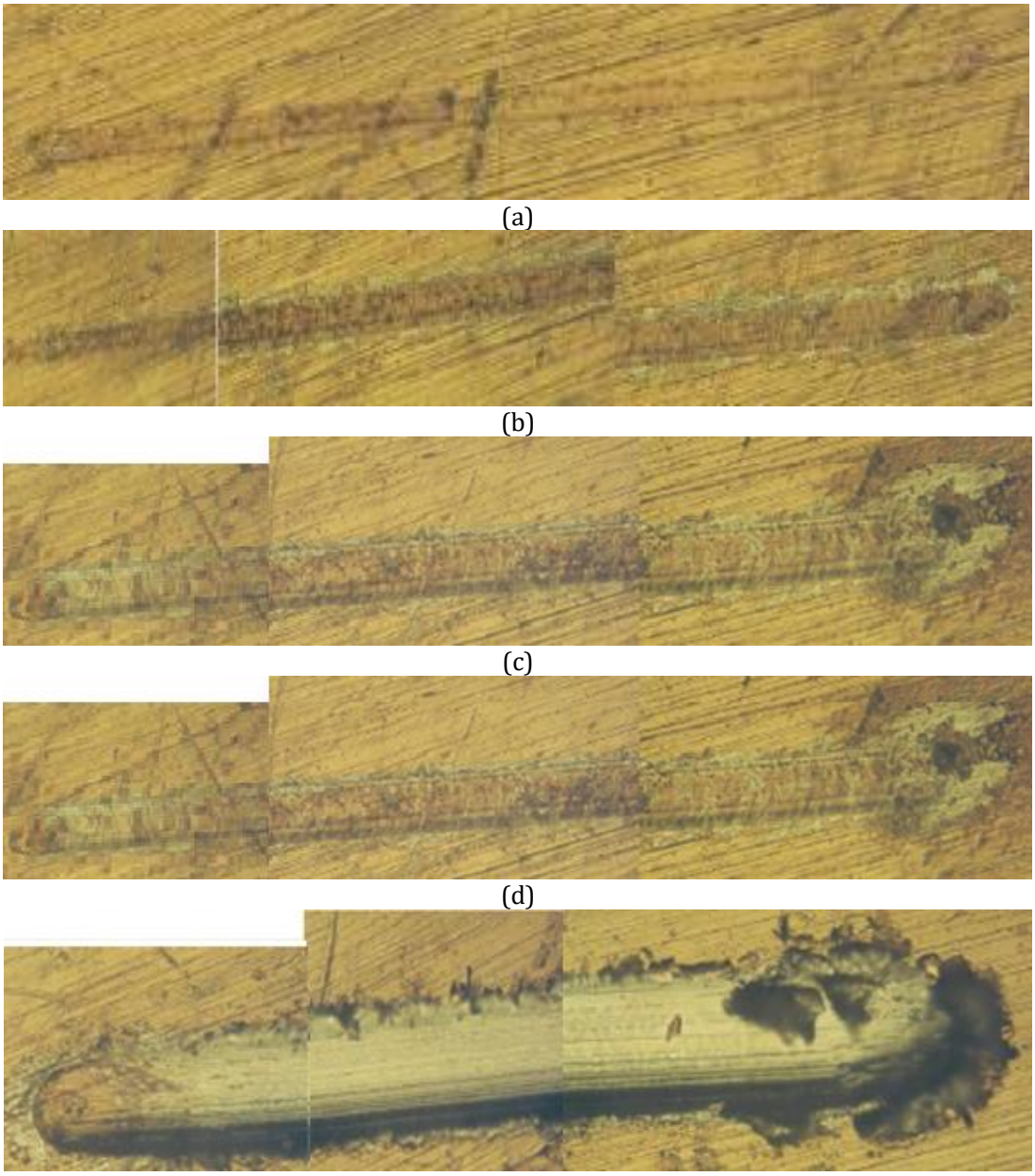

(a)

(b)

(c)

(d)

(e)

Figure 8: Collages of scratch tracks images taken at 2.5 N (a), 5 N (b), 10 N (c), 20 N (d), 40 N (e) and 80 N loads on coating at 10000 pulses.

Analyzing the images presented in Figures 7 and 8 of the scratches made on TiN PLD coating deposited on SS 316L substrate at 10000 pulses, the same findings can be made, but with some observations. The thickness of the TiN coating is 2.11 μm, with a hardness of 420 $HV_{0.5}$. Thus, although there are the same critical events – delamination on the edges of the scratch, sinking in at the beginning of the scratch and piling up at the end of it, their intensity is lower. The delaminated material and transferred to the sides of the scratch is more compact and in much smaller amount. At 80 N, the TiN coating at 10000 pulses was completely removed.

The plowing effect, obvious at the 5000 pulses coating, has now a tendency for transition to pure plowing. This could be explained by the higher tenacity of the coating. The pile up from the end of the scratch is obviously much lower and is made up of debris larger than at 5000 pulses, fact which could be explained by the same higher tenacity. The same explanation may also be for the appearance of the numerous dimples on the bottom of the scratches. The appearance of these dimples shows a tendency to pull out the coating material at the interface with the indenter that is moving and is under load. If these observations are associated with the appearance on the bottom of the scratch of some semicircular tracks, these could induce the idea of a stick-slip phenomenon between the indenter and the coating, but which only occurs up to the 40 N load. For scratch loads greater than 40 N, tendency for transition of the plowing to pure plowing appears, the bottom of the scratches becoming uniform, and their edges also uniform.

Making a comparison with the qualitative images recorded on scratches from the PLD coating at 5000 pulses, it is clear that the influence of increasing the coating's thickness, its hardness, as well as the hardness of the coating – substrate composite, has a beneficial influence on the scratch resistance of the coating. Figure 9 shows the scratch tests made on the 20000 pulses coating.

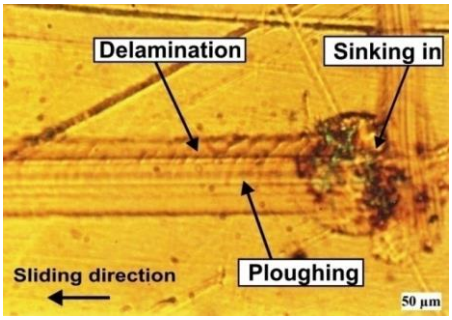

20000 pls, F = 2.5 N, track 1, start

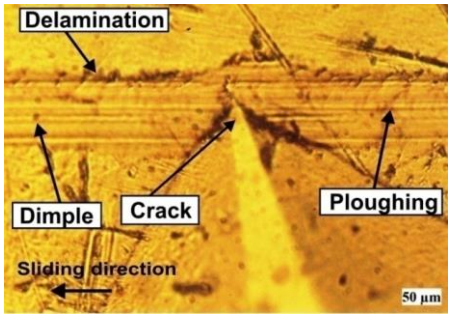

20000 pls, F = 2.5 N, track 1, pathway

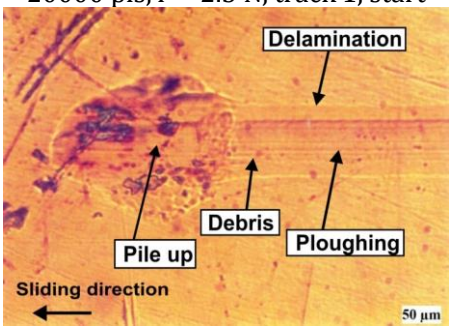

20000 pls, F = 2.5 N, track 1, final

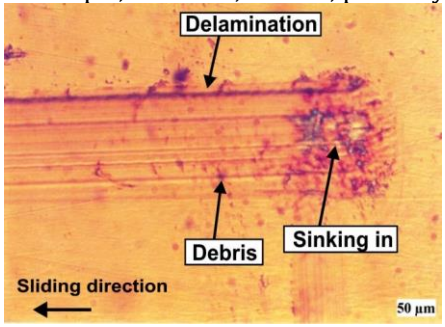

20000 pls, F = 5 N, track 2, start

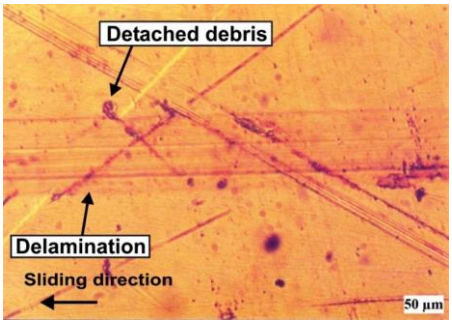

20000 pls, *F* = 5 N, track 2, pathway

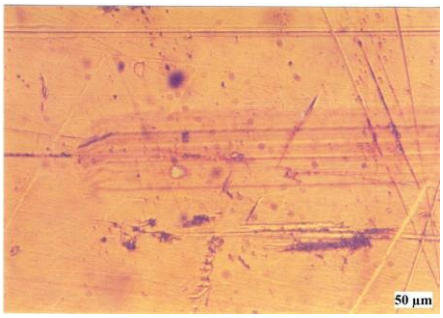

20000 pls, *F* = 5 N, track 2, final

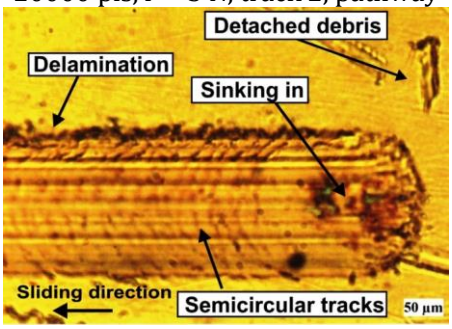

20000 pls, *F* = 10 N, track 3, start

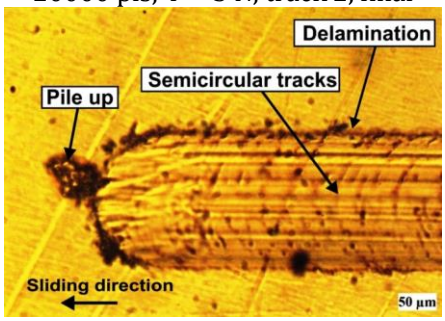

20000 pls, *F* = 10 N, track 3, final

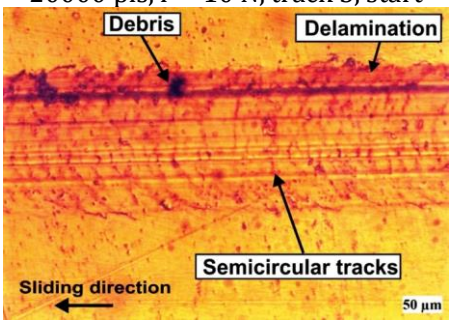

20000 pls, *F* = 10 N, track 3, pathway

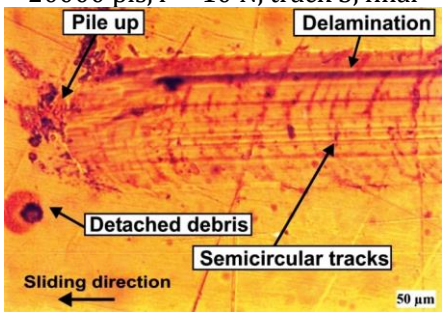

20000 pls, *F* = 10 N, track 3, final

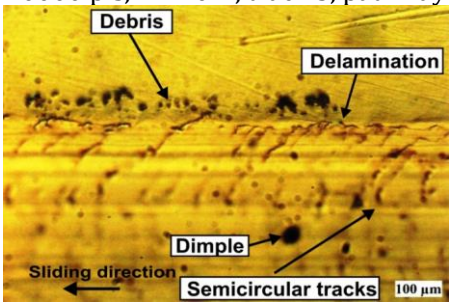

20000 pls, *F* = 10 N, track 3, pathway

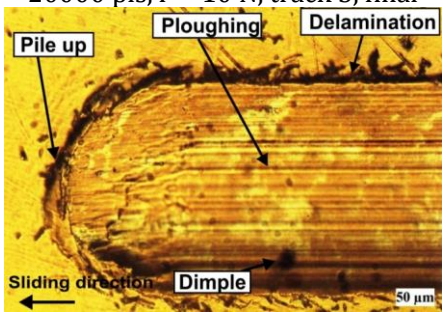

20000 pls, *F* = 20 N, track 4, final

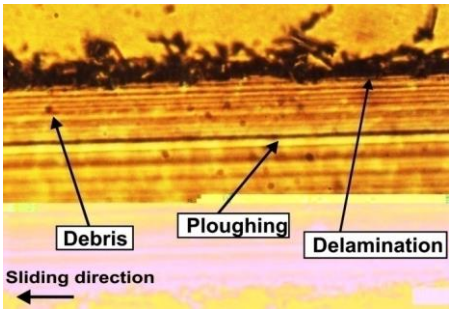

20000 pls, *F* = 20 N, track 4, pathway

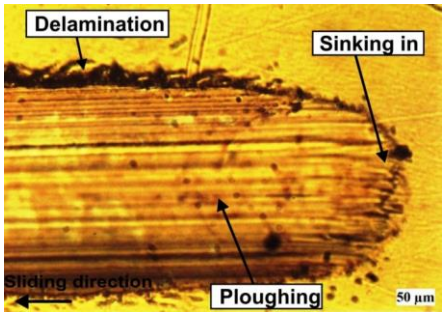

20000 pls, *F* = 20 N, track 4, start

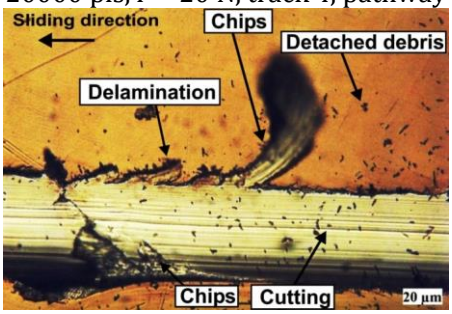

20000 pls, *F* = 40 N, track 5, pathway

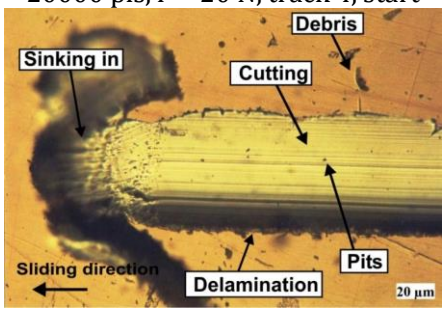

20000 pls, *F* = 40 N, track 5, start

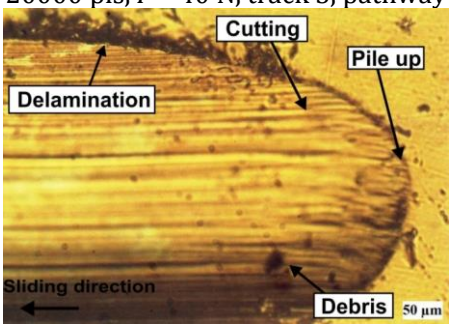

20000 pls, *F* = 40 N, track 5, final

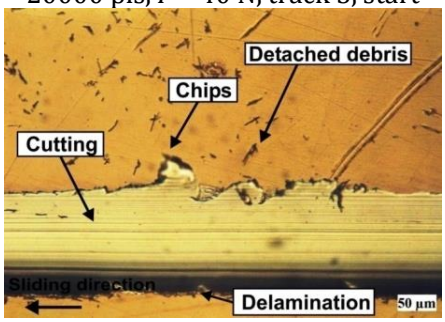

20000 pls, *F* = 40 N, track 5, pathway

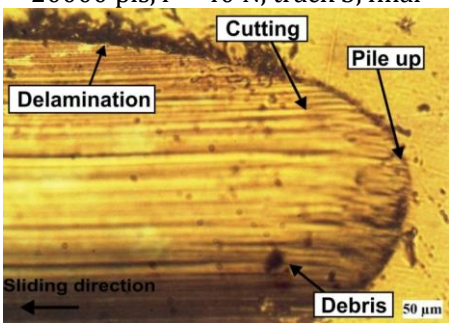

20000 pls, *F* = 40 N, track 5, final

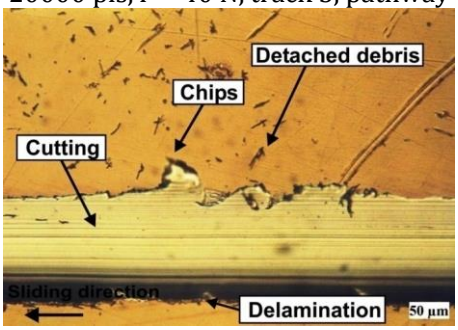

20000 pls, *F* = 40 N, track 5, pathway

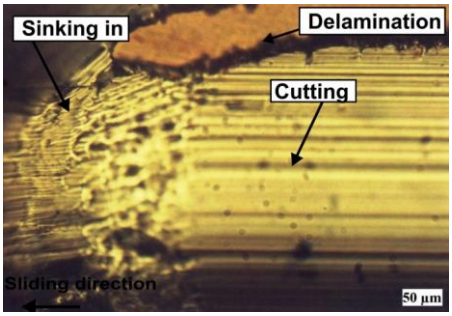

20000 pls, , F = 40 N, track 5, final

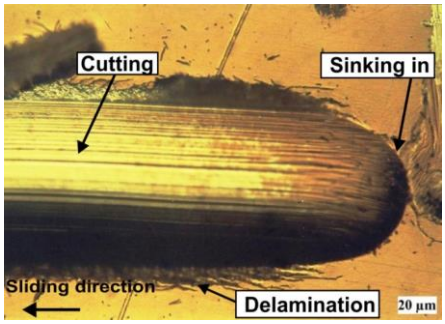

20000 pls, F = 80 N, track 6, final

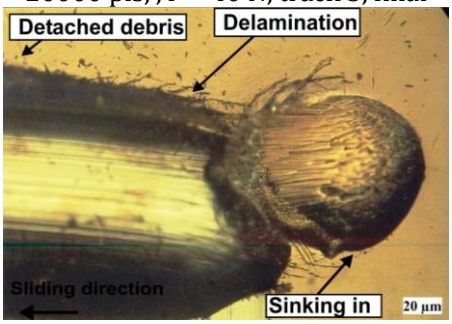

20000 pls, F = 125 N, track 7, start

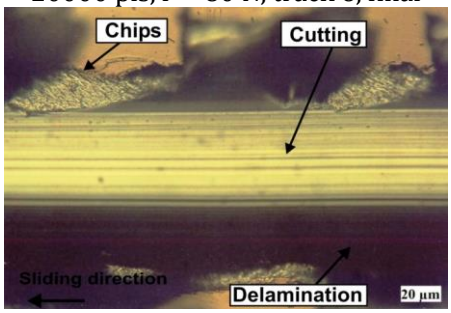

20000 pls, F = 125 N, track 7, pathway

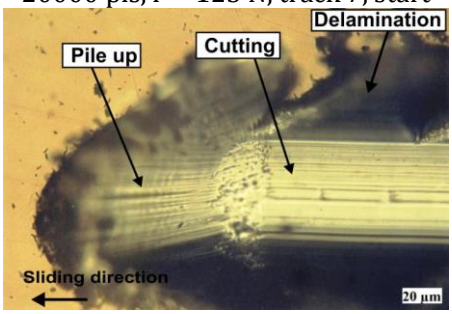

20000 pls, F = 125 N, track 7, final

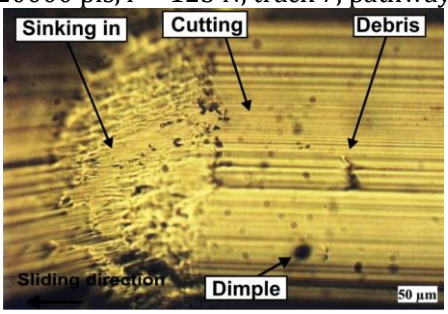

20000 pls, F = 125 N, track 7, start detail

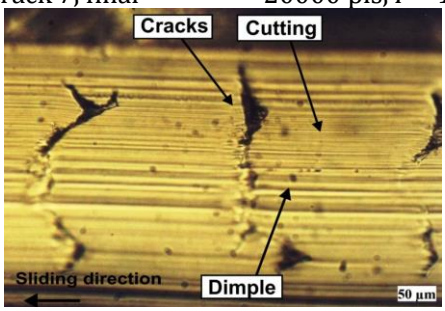

20000 pls, F = 125 N, track 7, pathway

Figure 9: Microscopic images of the tracks produced after the scratch tests for the 20000 pulses sample.

As it can be seen from the images presented in Figure 9, in the case of TiN coating at 20000 pulses, scratches could be made up to a load of 125 N, when the coating was completely removed,

unlike the TiN coatings at 5000 pulses and 10000 pulses, where the coating was completely removed at the scratch load of just 40 N, and 80 N, respectively.

Piling up from the end of the scratches is reduced and is made up of small scale debris, fact that could be explained by the very large microhardness (738 $HV_{0.5}$) of the PLD coating at 20000 pulses, confirming the findings of Gore and Gates (1997). The same explanation can also be considered for the appearance of the numerous dimples on the bottom of the scratches as well as the pits. The presence of dimples and pits shows a tendency to pull out the coating's material at the interface with the indenter that is moving and is under load, as a result of the very large contact efforts.

Also, appearance of cracks on the bottom of the scratches has to be observed, cracks that can indicate the start of the fatigue phenomena. If these observations are associated with the appearance on the bottom of the scratch of the semicircular tracks, also noted at the PLD coating at 10 pulses, these could induce the idea of a stick-slip phenomenon between the indenter and the coating. At scratching loads greater than 40 N, removing the material by plowing is replaced with the removal of the material by cutting, the bottom of the scratches becoming uniform, and their edges uniform, giving the impression of a classical cutting process.

Figure 10 shows collages of the scratch trakcs images made at loads of 2.5 N, 5 N, 10 N, 20 N, 40 N, 80 N and 125 N on TiN coating at 20000 pulses.

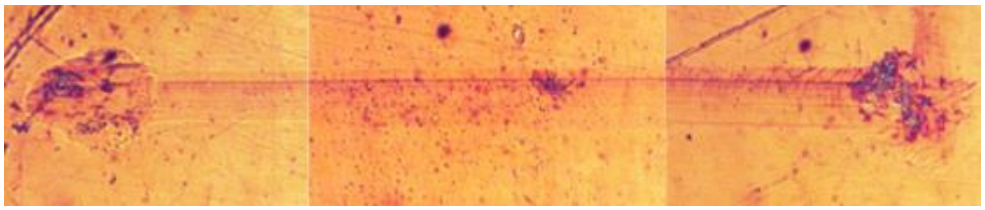

(a)

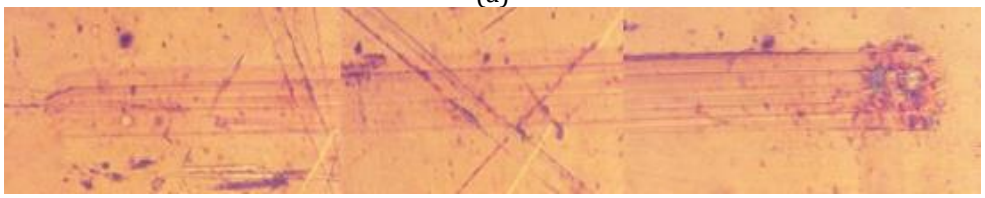

(b)

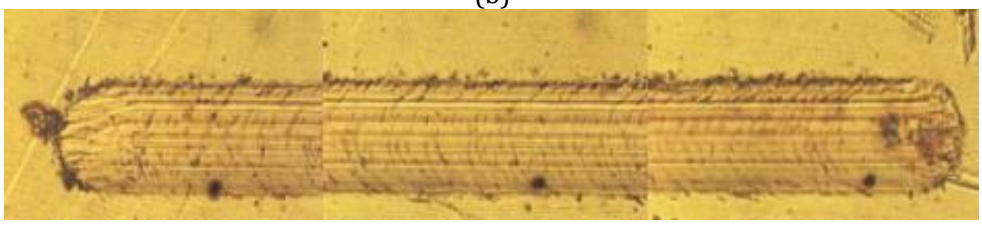

(c)

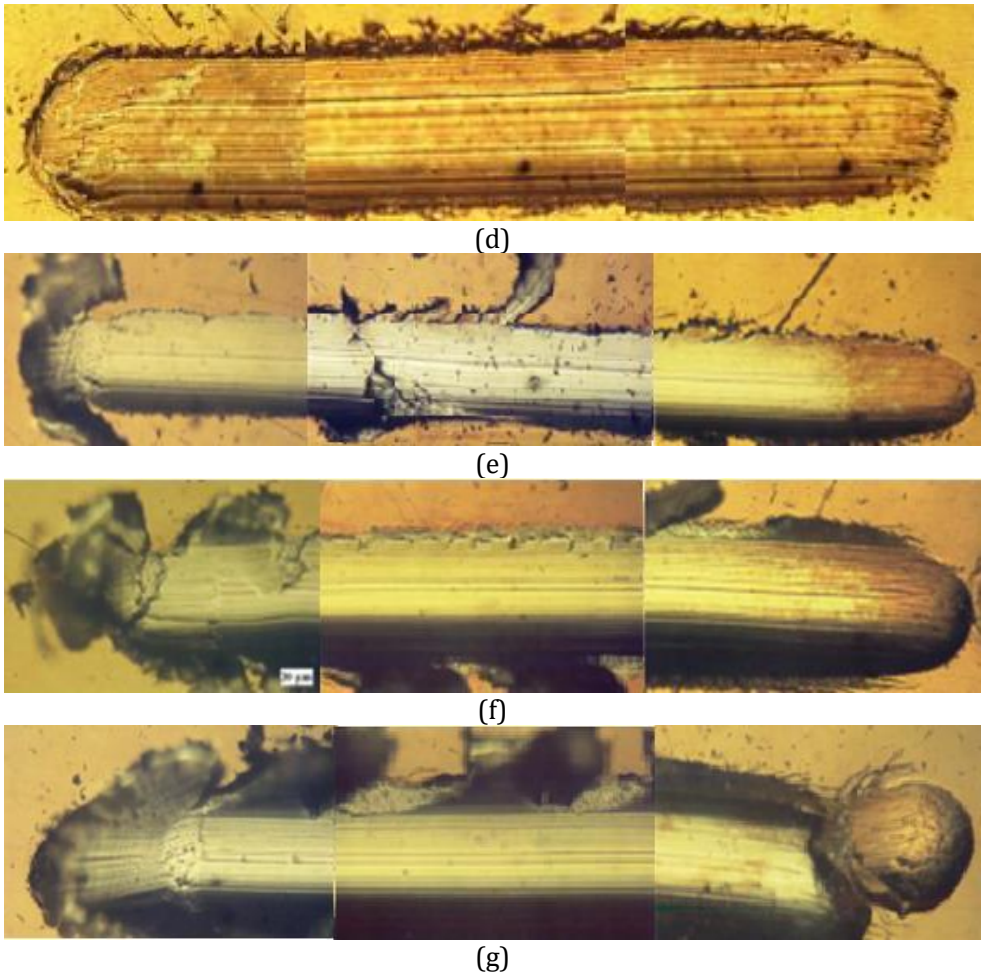

(d)

(e)

(f)

(g)

Figure 10: Collages of scratch tracks images taken at 2.5 N (a), 5 N (b), 10 N (c), 20 N (d), 40 N (e), 80 N and 125 N (g) loads on coating at 20000 pulses.

Collages shown in Figures 6, 8 and 10 provide suggestive images of the complexity of the failure mechanisms evolution of the TiN coatings on SS 316L stainless steel substrates. Three types of TiN coatings were realized on cylindrical samples of SS 316L by Pulse Laser Deposition (PLD). Depending on the number of deposition pulses, coatings with different thicknesses and different hardnesses were obtained. Because the failure of coatings with thin layers is generally due to the failure of coating's adhesion to the substrate's material, the coating's adhesion was tested by single pass single indenter (SPSI) scratch tests to completely avoid the appearance of the fatigue phenomenon that may occur in the case of multi-pass single indenter (MPSI) scratch test or multi-pass dual indenters (MPDI).

The wear mechanism is continually evolving, from delamination and debris formation to plowing and cutting. The cutting wear mechanism only manifests itself in the PLD coating at 20000 pulses, accompanied by the enhancement of the stick-slip motion of the indenter on the scratch track, highlighted by intense semicircular tracks on the bottom of the scratch.

PLD coating with TiN deposited at 5000 pulses was completely removed at the 40 N scratch load, while the TiN coating at 10000 pulses was completely removed at 80 N, causing the scratch tests interruption. TiN coating at 20000 pulses resisted up to 125 N. It is possible that for one scratch, the wear mechanism to be changed from plowing to cutting, due to the interaction of parallel scratches. It is also possible that parallel scratches to have been interacted due to the proximity (overlapping), therefore micro-plowings combined with the formation of shavings at the edge of the scratches were presented, confirming the report of Da Silva et al. (2011), according to which this wear mechanism is intermediate between micro-plowing and micro-cutting, showing deformed material and small shavings on the scratch sides. The wear debris near the end part of the parallel scratches have a similar form to the shavings formed on the sides of the scratches. Again, a transition mechanism of the wear could be detected, from micro-plowing to micro-cutting due to the overlapping degree of the parallel scratches interactions.

CONCLUSION

(a) This paper has attempted to provide a qualitative image of the failure mechanisms of the TiN coatings deposited on substrates made of SS 316L.
(b) The critical failure events of the three types of coatings were highlighted and commented, concluding that PLD coatings with 10000 and 20000 pulses are the ones that offer the most favorable perspectives from the coating – substrate adhesion point of view.
(c) Critical events involve the delamination of the coating, the massive appearance of wear debris, the appearance of semicircular tracks on the bottom of the scratches, as well as the dimples and pits, probably signs of stick-slip motion.
(d) PLD coating with TiN deposited at 20000 pulses proved to be the most scratch resistant, probably due to the 738 $HV_{0.5}$ microhardness of the coating, and the 464 $HV_{0.5}$ hardness of the substrate, confirming the findings on the influence of hardness of Gore and Gates (1997).

REFERENCES

Avelar-Batista, J. C., Spain, E., Fuentes, G. G., Sola, A., Rodriguez, R., & Housden, J. (2006). Triode plasma nitriding and PVD coating: A successful pre-treatment combination to improve the wear resistance of DLC coatings on Ti6Al4V alloy. Surface and Coatings Technology, 201(7), 4335-4340.

Büscher, R., Täger, G., Dudzinski, W., Gleising, B., Wimmer, M. A., & Fischer, A. (2005). Subsurface microstructure of metal‐on‐metal hip joints and its relationship to wear particle generation. Journal of Biomedical Materials Research Part B: Applied Biomaterials, 72(1), 206-214.

Capitanu, L., Badita, L. L., Tiganesteanu, C., & Rus, D. (2015). Scratch and cyclic impact testing of adhesion PLD coatings, Ti-N on SS316L substrate. Cemented Carbide, 4(9), 78-107.

Cawley, J., Metcalf, J. E. P., Jones, A. H., Band, T. J., & Skupien, D. S. (2003). A tribological study of cobalt chromium molybdenum alloys used in metal-on-metal resurfacing hip arthroplasty. Wear, 255(7-12), 999-1006.

Chelliah, N., & Kailas, S. V. (2009). Synergy between tribo-oxidation and strain rate response on governing the dry sliding wear behavior of titanium. Wear, 266(7-8), 704-712.

Coll, B., Pellman, M. A., Souchard, J. P., & Jarquot, P. (1998). Metallurgical and Tribological Modification of Titanium and Titanium Based Alloys for Medical Devices by Plasma Assisted Techniques. Technical Bulletin from Multi-Arc Scientific Coatings/Innovatique SA.

Da Silva, W. M., Costa, H. L., & De Mello, J. D. B. (2011). Transitions in abrasive wear mechanisms: Effect of the superimposition of interactions. Wear, 271(5-6), 977-986.

Dobbs, H. S., & Robertson, J. L. M. (1983). Heat treatment of cast Co-Cr-Mo for orthopaedic implant use. Journal of Materials Science, 18(2), 391-401.

Fouquet, V., Pichon, L., Straboni, A., & Drouet, M. (2004). Nitridation of Ti6Al4V by PBII: study of the nitrogen diffusion and of the nitride growth mechanism. Surface and Coatings Technology, 186(1-2), 34-39.

Gore, G. J., & Gates, J. D. (1997). Effect of hardness on three very different forms of wear. Wear, 203, 544-563.

Hiromoto, S., Onodera, E., Chiba, A., Asami, K., & Hanawa, T. (2005). Microstructure and corrosion behaviour in biological environments of the new forged low-Ni Co–Cr–Mo alloys. Biomaterials, 26(24), 4912-4923.

Holmberg, K. (1992). A concept for friction mechanisms of coated surfaces. Surface and Coatings Technology, 56(1), 1-10.

Holmberg, K., Matthews, A., & Ronkainen, H. (1998). Coatings tribology—contact mechanisms and surface design. Tribology International, 31(1-3), 107-120.

Jacobs, J. J., Latanision, R. M., Rose, R. M., & Veeck, S. J. (1990). The effect of porous coating processing on the corrosion behavior of cast Co–Cr–Mo surgical implant alloys. Journal of Orthopaedic Research, 8(6), 874-882.

Julian, L. C., & Munoz, A. I. (2011). Influence of microstructure of HC CoCrMo biomedical alloys on the corrosion and wear behaviour in simulated body fluids. Tribology International, 44(3), 318-329.

Kustas, F. M., & Misra, M. S. (2007). Friction and wear of titanium alloys, in: ASM Handbooks online, vol.18, Friction, Lubrication, and Wear Technology, ASM International.

Lanning, B. R., & Wei, R. (2004). High intensity plasma ion nitriding of orthopedic materials: Part II. Microstructural analysis. Surface and Coatings Technology, 186(1-2), 314-319.

Liu, C., Bi, Q., & Matthews, A. (2003). Tribological and electrochemical performance of PVD TiN coatings on the femoral head of Ti–6Al–4V artificial hip joints. Surface and coatings Technology, 163, 597-604.

Liu, X., Chu, P. K., & Ding, C. (2004). Surface modification of titanium, titanium alloys, and related materials for biomedical applications. Materials Science and Engineering: R: Reports, 47(3-4), 49-121.

Meletis, E. I., Erdemir, A., & Hochman, R. F. (1986). Ion Plating and Implantation Applications to Materials. American Society for Metals, Metals Park, OH, 173.

Molinari, A., Straffelini, G., Tesi, B., Bacci, T., & Pradelli, G. (1997). Effects of load and sliding speed on the tribological behaviour of Ti · 6Al · 4V plasma nitrided different temperatures. Wear, 203, 447-454.

Österle, W., Klaffke, D., Griepentrog, M., Gross, U., Kranz, I., & Knabe, C. (2008). Potential of wear resistant coatings on Ti–6Al–4V for artificial hip joint bearing surfaces. Wear, 264(7-8), 505-517.

Pellman, M. (2000). PVD Coatings for Medical Device Applications. Products Finishing, 64(10), 116-121.

Rie, K. T., Stucky, T., Silva, R. A., Leit, E., Bordji, K., Jouzeau, J. Y., & Mainard, D. (1995). Plasma surface treatment and PACVD on Ti alloys for surgical implants. Surface and Coatings Technology, 74, 973-980.

Rodrigues, W. C., Broilo, L. R., Schaeffer, L., Knörnschild, G., & Espinoza, F. R. M. (2011). Powder metallurgical processing of Co–28% Cr–6% Mo for dental implants: Physical, mechanical and electrochemical properties. Powder Technology, 206(3), 233-238.

Santos, L. V., Trava-Airoldi, V. J., Corat, E. J., Nogueira, J., & Leite, N. F. (2006). DLC cold welding prevention films on a Ti6Al4V alloy for space applications. Surface and Coatings Technology, 200(8), 2587-2593.

Schutz, R. W. (2005). Corrosion of titanium and titanium alloys. ASM Handbook, Vol. 13 B, Corrosion: Materials, 13, 252-299.

Sims, C. (1972). *Cobalt based alloys*. New York: JohnWiley & Sons.

Tanno, Y., & Azushima, A. (2009). Effect of counter materials on coefficients of friction of TiN coatings with preferred grain orientations. Wear, 266(11-12), 1178-1184.

Varenberg, M., Halperin, G., & Etsion, I. (2002). Different aspects of the role of wear debris in fretting wear. Wear, 252(11-12), 902-910.

Vidal, C. V., & Muñoz, A. I. (2008). Electrochemical characterisation of biomedical alloys for surgical implants in simulated body fluids. Corrosion Science, 50(7), 1954-1961.

Wilson, A. D., Leyland, A., & Matthews, A. (1999). A comparative study of the influence of plasma treatments, PVD coatings and ion implantation on the tribological performance of Ti–6Al–4V. Surface and coatings technology, 114(1), 70-80.

Yilbas, B. S., Sahin, A. Z., Ahmad, Z., & Aleem, B. A. (1995). A study of the corrosion properties of TiN coated and nitrided Ti-6Al-4V. Corrosion Science, 37(10), 1627-1636.

Yilbaş, B. S., Şahin, A. Z., Al-Garni, A. Z., Said, S. A., Ahmed, Z., Abdulaleem, B. J., & Sami, M. (1996). Plasma nitriding of Ti6Al4V alloy to improve some tribological properti. Surface and Coatings Technology, 80(3), 287-292.

Zhang, Z. X., Dong, H., Bell, T., & Xu, B. S. (2008). The effect of deep-case oxygen hardening on the tribological behaviour of aC: H DLC coatings on Ti6Al4V alloy. Journal of Alloys and Compounds, 464(1-2), 519-525.

Zhou, Z., Rainforth, W. M., Tan, C. C., Zeng, P., Ojeda, J. J., Romero-Gonzalez, M. E., & Hovsepian, P. E. (2007). The role of the tribofilm and roll-like debris in the wear of nanoscale nitride PVD coatings. Wear, 263(7-12), 1328-1334.